Response of copper nanowires in dynamic tensile deformation

W Liang and **M Zhou***
The Woodruff School of Mechanical Engineering, Georgia Institute of Technology, Atlanta, Georgia, USA

Abstract: Molecular dynamics (MD) simulations with an embedded atom method (EAM) potential are carried out to analyse the size and strain rate effects in the tensile deformation of single-crystal copper nanowires. The cross-sections of the wires are squares with dimensions of between 5 and 20 lattice constants (or 1.8–7.2 nm). Deformations under constant strain rates between 1.67×10^7 and $1.67 \times 10^{10}\,s^{-1}$ are analysed. It is found that the yield stress decreases with specimen size and increases with loading rate. On the other hand, ductility increases with specimen size and strain rate. The influence of specimen size is due to enhanced opportunities for dislocation motion at larger sizes. The influence of strain rate is due to the dynamic wave effect or phonon drag which impedes the motion of dislocations. The analysis also focuses on the variation in deformation mechanisms with specimen size and strain rate. Slip along alternating (111) planes is observed in small wires, while multiple cross-slips are primarily responsible for the progression of plastic deformation in larger wires. As strain rate is increased, a transition of the deformation mechanism from sequential propagation of slip along well-defined and favourably oriented slip planes to cross-slip, and then to amorphization, is observed.

Keywords: molecular dynamics, nanowire, size effect, rate effect, slip, amorphization

1 INTRODUCTION

The deformation of nanowires and atomic systems at finite temperatures in general is an intrinsically dynamic process. Size and strain rate effects arise out of several factors and play important roles in determining the response of nanostructures. For example, the behaviour and properties of nanowires are size dependent owing to the discreteness of atomic structures, the length scale (or spatial range) of the atomic interactions, lattice structure and lattice size scale. The dynamic inertia effect and the finite speeds at which lattice waves propagate also introduce length scales to the problem and contribute to the size dependence of atomic behaviour. The inertia effect and finite wave speeds, along with phonon effects, also cause the response of nanostructures to be deformation rate dependent.

Experimental and numerical studies on the deformation of nanowires have been carried out and reported in recent years {**1**–**5**}. For example, Lu *et al.* {**6**} observed that the ductility of nanocrystalline copper specimens increases as strain rate increases in experiments. This strain rate dependence of ductility is completely different from that observed in coarse-grained Cu, the fracture strain of which decreases with increasing strain rate. Ikeda *et al.* {**2**} and Bran;cio and Rino {**7**} used molecular dynamics (MD) simulations to study the amorphization in metallic nanowires at high strain rates. They found that, at strain rates lower than $7 \times 10^{10}\,s^{-1}$, the nanowires undergo plastic deformation in their crystalline structure and exhibit superplasticity. On the other hand, at strain rates equal to or higher than $7 \times 10^{10}\,s^{-1}$, the nanowires undergo a phase transition from a crystalline structure to an amorphous state. Horstemeyer and Baskes {**8**} analysed the effects of size and time-scale on the plastic deformation of bulk single-crystal Cu under shear loading. They found that samples with less than ~ 1000 atoms showed little dependence of failure stress on strain rate. This is because small samples do not provide opportunities for plastic deformation to occur through coordinated slip or dislocation motion. Consequently, the deformation is primarily elastic. On the other hand, for larger samples

The MS was received on 27 May 2003 and was accepted after revision for publication on 28 October 2003.
* *Corresponding author: The Woodruff School of Mechanical Engineering, Georgia Institute of Technology, Atlanta, GA 30332-0405, USA.*

they found that, at relatively low strain rates, the yield stress is independent of strain rate, while at higher strain rates the yield stress increases rapidly with strain rate. This effect is attributed to the fact that multiple dislocations are nucleated at the lower rates, lowering the yield stress. They also asserted that four regions of bulk plastic behaviour exist, depending on the size scale. As the size scale increases, there is a gradual change in influence on plastic behaviour from dislocation nucleation at much smaller scales to dislocation density and distribution at larger scales.

Up till now, MD calculations of the mechanical response of atomic systems have been almost exclusively carried out at strain rates above $10^9 s^{-1}$. This is primarily out of necessity. Specifically, the time steps allowable in MD calculations are limited by the need to resolve high-frequency thermal oscillations of atoms and are therefore quite small (of the order of 1 fs). High rates of deformation allow high levels of strain to be reached with practically available computer resources. The use of high deformation rates introduces several issues. Firstly, direct comparisons with experiments are extremely difficult to justify since it is so far not possible to conduct controlled laboratory experiments at high strain rates on nanowires or nanostructures. The artificially high rates have also necessitated computational schemes that allow computations to proceed. One issue is temperature control. Many MD simulations of nanowires have been carried out with the Nose–Hoover thermostat scheme {**9**, **10**}, a velocity scaling scheme that keeps the temperature at constant values. If such schemes were not used, the artificially high strain rates could lead to temperatures well over the melting point of the system under consideration, invalidating the results and preventing analyses to be carried out. The use of such schemes has allowed results to be obtained and important understandings to be arrived at. However, it is also desirable and important to conduct numerical simulations under conditions that allow the temperature to increase as a natural outcome of dynamic deformation. Here, it is noted that, while MD models account for the contribution of atomic vibrations (or phonons) to thermal conductivity, they do not account for the effects of free electrons, electron/phonon interactions and bipolar carriers. This is a limitation of the MD framework. Accounting for such effects would require modifications to the MD framework, if classical mechanics were to be used. There have been efforts to carry out simulations at lower strain rates. Recent calculations at strain rates between 10^7 and $10^{10} s^{-1}$ are described here. No temperature-controlling algorithms are used, providing a more realistic account of the conditions of the dynamic deformation of nanowires. The focus of the analyses is on the size and rate effects on the constitutive response of Cu nanowires. Parameters varied include loading rate and specimen size.

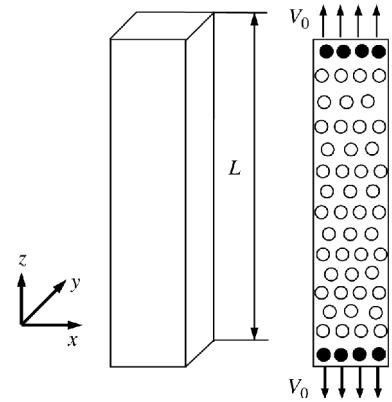

Fig. 1 Schematic illustration of the computational model for Cu nanowires. Open circles represent the internal atoms and dark circles represent boundary atoms

2 COMPUTATIONAL SET-UP

The MD simulations carried out concern the simple tension of single-crystal Cu nanowires (see Fig. 1). The nanowires have free surfaces in the x and y directions. The x, y and z axes are oriented in the {100}, {010} and {001} crystalline directions respectively. The atoms in the specimens are divided into two types. The first type consists of boundary atoms on the top and bottom surfaces. Constant velocities of $\pm V_0$ (equal magnitude and opposite directions) are maintained for these two planes of atoms, effecting the loading necessary for the nanowire to deform at a constant nominal strain rate $\dot{\varepsilon} = 2V_0/L$. The internal atoms simply deform with the boundary atoms. Although dynamic in nature, this set of loading conditions yield fairly uniform deformation throughout the specimen. Localization or necking always occurs in the interior of the wires, away from the ends. The location of the neck is fairly randomly distributed along the wire length in different specimens. The system is assigned an initial temperature of 300 K and is allowed to reach a uniform thermal state by holding the length of the wire unchanged and by maintaining a constant temperature using the Nose–Hoover thermostat procedure. The nanowires are not relaxed to a zero stress state, and the beginning of deformation is at stress levels of 0.4–1.6 GPa, depending on the wire size. The calculations are carried out with a time step of 1 fs until fracture occurs. In contrast to some MD simulations reported in the literature where the Nose–Hoover thermostat procedure was used to maintain a constant temperature, no thermal constraints are applied to the specimen during the calculations here. Therefore, the temperature rises adiabatically. This treatment more closely simulates the tensile deformation of nanowires undergoing high-rate deformation.

3 RESULTS AND DISCUSSION

3.1 Strain rate effects

Figure 2 shows the stress–strain relations at strain rates between 1.67×10^7 and $1.67 \times 10^{10}\,s^{-1}$. The cross-sectional size of the wires here is 5 lattice constants (1.8×1.8 nm). These stress–strain relations are essentially linear at small strains, except for small thermal oscillations. The yield stress is the maximum stress in these cases. The curves for different strain rates essentially coincide during the elastic part of the deformation, indicating rate independence of elastic deformations, which is expected. The curves show a rate independent Young's modulus of 70 GPa for the $\langle 001 \rangle$ type crystalline directions. The yield stress is higher at higher strain rates, increasing from 6.8 to 7.8 GPa as the strain rate increases from 1.67×10^7 to $1.67 \times 10^{10}\,s^{-1}$. This rate dependence is due to the dynamic wave effect or phonon drag which impedes the motion of dislocations. Owing to the lack of defects and the surface effects, the yield stress for nanowires undergoing dynamic deformation exceeds that of bulk Cu.

The nanowire exhibits very different responses at strain rates below $1.67 \times 10^{10}\,s^{-1}$ from the response at the strain rate of $1.67 \times 10^{10}\,s^{-1}$. Specifically, the curves at strain rates below $1.67 \times 10^{10}\,s^{-1}$ show precipitous drops in stress after yielding. These sharp drops are associated with the initiation of plastic deformation which occurs through crystalline slip along [111] planes. This mechanism of deformation is clearly seen in Figs 3a and b. In contrast, stress decreases only gradually after the onset of inelastic deformation at a strain rate of $1.67 \times 10^{10}\,s^{-1}$. Furthermore, the wire shows a much higher level of ductility than those at the lower strain rates. This change in behaviour is due to a transition in the deformation mechanism from crystalline slip to amorphization (see Figs 3c and d). This observation of transition in the deformation mechanism is consistent with what was reported for metallic wires in the literature {2}. The significantly higher level of ductility is regarded as a form of superplasticity in nanowires.

At the strain rates of 1.67×10^7 and $1.67 \times 10^8\,s^{-1}$, activation of two alternating slip planes is observed (see Figs 3a and b). With loading in the {001} direction, eight slip systems initially have an identical Schmid factor and are 'equally' favoured for slip. These eight slip systems form four conjugate slip pairs, which compete with each other. The two slip systems actually activated are the primary slip system $(11\bar{1})[101]$ and its conjugate system $(1\bar{1}1)[110]$. The activation of only one pair of slip planes indicates the effects of available energy and thermal perturbation. The activation of one pair of conjugate slip systems suppresses others by the consumption of available energy. When the primary slip system is activated by thermal perturbation, the orientation of the tensile axis will rotate towards the slip direction.

However, since the tension axis is fixed in the simulation, it is the crystal lattice that undergoes the actual rotation. Hence, during the large tensile deformation, the slip direction will rotate towards the tensile axis. This rotation of slip planes lowers the Schmid factor for the primary slip system and increases the Schmid factor for its conjugate slip system, causing the conjugate system to be activated. Therefore, the activation of the two alternating slip systems allows the tensile axis to remain unchanged and relieves the shear stress at the same time.

Even though the final configurations of the activated slip planes look similar at strain rates of 1.67×10^7 and

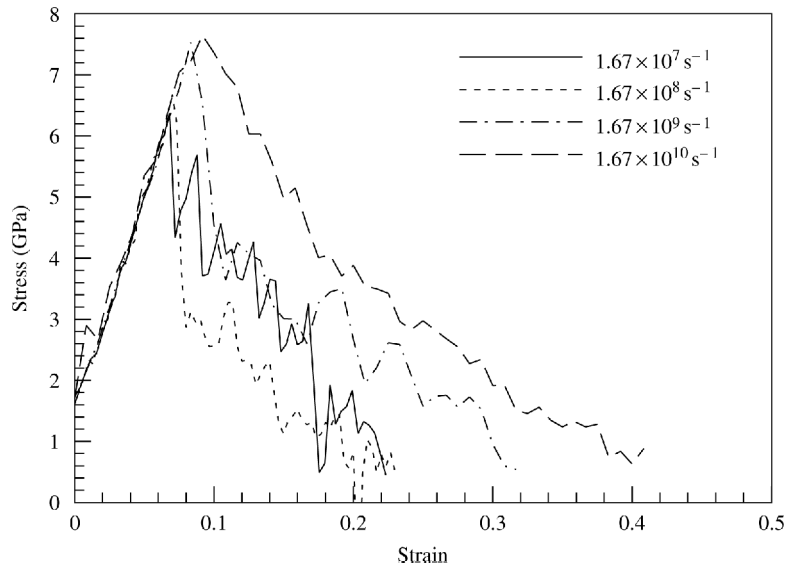

Fig. 2 Stress–strain curves of $5 \times 5 \times 60$ Cu nanowires at different strain rates

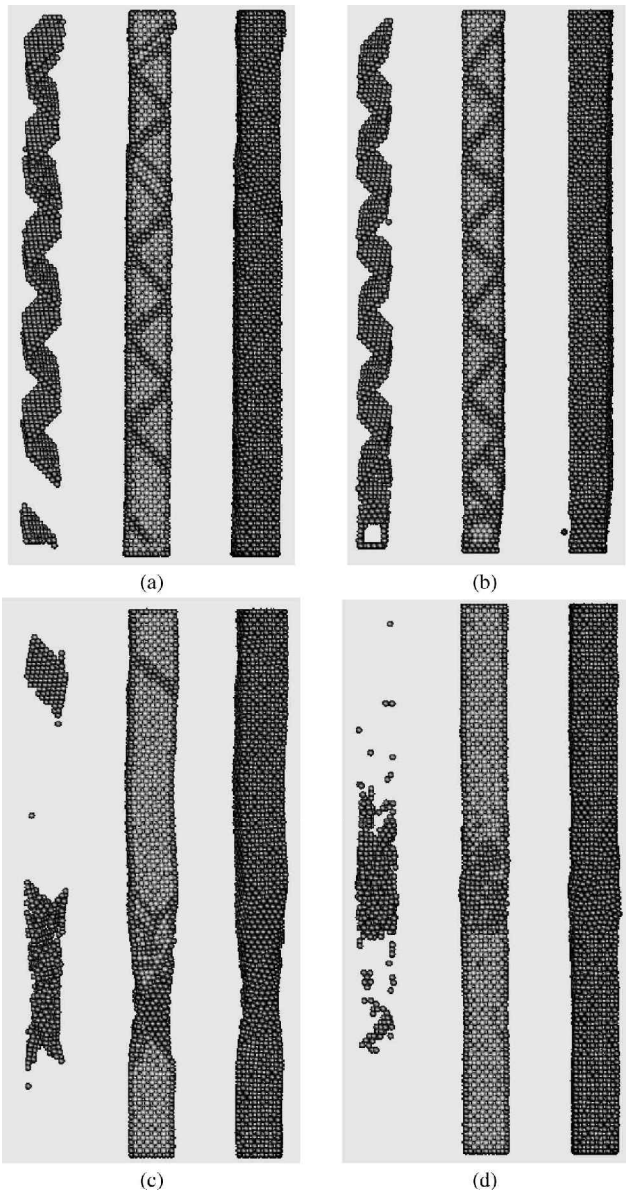

Fig. 3 Deformed configurations of Cu nanowires at a strain of 10 per cent: (a) $\dot{\varepsilon} = 1.67 \times 10^7\,\mathrm{s}^{-1}$; (b) $\dot{\varepsilon} = 1.67 \times 10^8\,\mathrm{s}^{-1}$; (c) $\dot{\varepsilon} = 1.67 \times 10^9\,\mathrm{s}^{-1}$; (d) $\dot{\varepsilon} = 1.67 \times 10^{10}\,\mathrm{s}^{-1}$. In each picture, the central image shows an internal cross-section, the right-hand image shows a solid view of the wire with all atoms and the left-hand image shows only atoms involved in defects. The atoms are shown according to their centrosymmetry values {**11**}

$1.67 \times 10^8\,\mathrm{s}^{-1}$, the processes of slip plane activation are quite different. The slip bands are nearly simultaneously activated at a strain rate of $1.67 \times 10^7\,\mathrm{s}^{-1}$, while they propagate from one end to the other within a certain period of time at a strain rate of $1.67 \times 10^8\,\mathrm{s}^{-1}$ (see Fig. 4). This apparent difference in the activation of slip systems is related to two different types of dislocation source and the effect of the stress wave.

The simultaneous, uniform activation of slip planes throughout the nanowire is observed at a strain rate of $1.67 \times 10^7\,\mathrm{s}^{-1}$. The wire is elastically stressed until uniform shifting along an atomic plane occurs. This process generates two dislocations that move in opposite directions. Initially, only scattered, discrete sites of higher lattice distortion are nucleated on alternating (111) planes along the wire. Subsequently, the density of such sites increases, leading to activation of slip planes. The activation is accompanied with precipitous drops in stress. In contrast, the sequential activation of slip at a strain rate of $1.67 \times 10^8\,\mathrm{s}^{-1}$ is quite different and is characterized by the nucleation of dislocations from the specimen surface. Specifically, dislocations are initially nucleated from a corner at one end of the wire where the highest lattice distortion occurs owing to boundary constraint (see Fig. 4a). This nucleation of dislocation sets off a successive, chain reaction type activation of slip planes along the specimen. Figure 5 shows the histories of the distance of propagation and the velocity of the active front of the slip planes corresponding to the wire in Fig. 4. The average speed at which the active front propagates along the wire is 355 m/s. The instantaneous speed oscillates between zero and a maximum of the order of 1000 m/s. This oscillation is associated with the transition of the propagating front between slip planes. The level of the speeds observed here constitutes significant fractions of stress wave speeds in Cu. In particular, note that the stress wave speed in the $\langle 001 \rangle$ direction of single-crystal copper is 2092 m/s for uniaxial stress and 4198 m/s for uniaxial strain. The rapid activation of slip planes across the specimen is responsible for the near-vertical drop in stress following yielding in Fig. 2 for this strain rate.

Following initial yielding, the stress–strain curves for strain rates between 1.67×10^7 and $1.67 \times 10^9\,\mathrm{s}^{-1}$ show oscillatory decreases in stress after the onset of plastic deformation. These oscillations are probably due to successive stages of gradual elastic stretching of temporarily 'stationary' lattice structures and rapid plastic slip along the well-defined slip planes. This is evidenced by the stepwise decrease in neck area during the necking process (see Fig. 6). This unique necking process has been observed in experiments, in which the neck area is obtained by measuring conductance of the nanowire {**12**}. During the relatively 'elastic' stages of deformation after yielding, the neck area remains relatively constant and straining of the lattice allows strain energy to be accumulated and stored. The stored strain energy allows the activation of slip planes in short, 'quick-fire' bursts, leading to relaxation and drops in stress as strain increases. Meanwhile, the neck area drops quickly as a new layer is generated. Since specimens deforming at lower strain rates need longer times to 'catch up' through further 'elastic' straining, stress decreases are sharper and last a longer time.

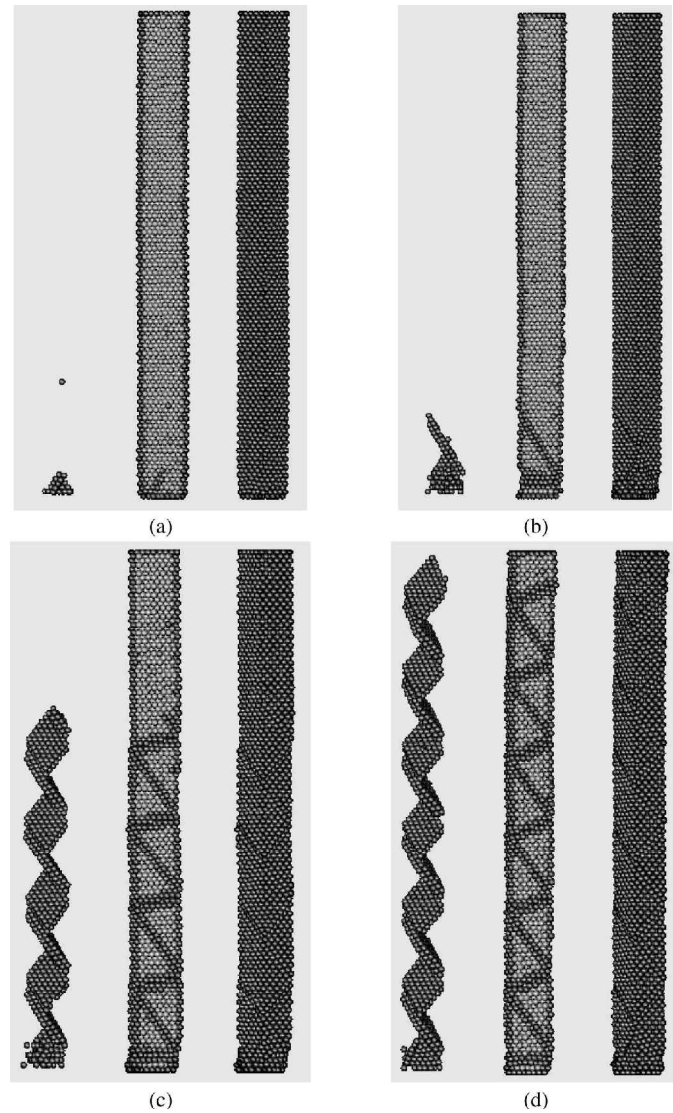

Fig. 4 Propagation of dislocations at a strain rate of $1.67 \times 10^8\ s^{-1}$: (a) $\varepsilon = 4.2$ per cent; (b) $\varepsilon = 4.67$ per cent; (c) $\varepsilon = 5.33$ per cent; (d) $\varepsilon = 6.0$ per cent. Specimen size $5 \times 5 \times 60$

3.2 Size scale effects

Figure 7 shows the stress–strain curves for specimens of three different sizes at a strain rate of $1.67 \times 10^9\ s^{-1}$. The cross-sectional dimensions vary from 5 to 20 lattice constants (or from 1.8 to 7.2 nm) and the length is 60 lattice constants (21.7 nm) in all cases. Thinner wires support higher stresses, and the yield stress decreases with specimen size. The Young's modulus remains essentially the same for the different sizes, as the initial elastic portions of the stress–strain curves are essentially parallel to each other. This size independence of the Young's modulus is different from the findings of Bran;cio who reported that nanowires with larger cross-sections support higher stress levels and have higher values of the Young's modulus {**13**}. The different amounts of initial stress are due to the uniform prestretch applied to the specimens prior to the start of the deformation process and due to the free surface effect. Only a small portion of the atoms in the thinnest wire are involved in the plastic deformation. Therefore, the deformation is rather non-uniform along the wire. As the wire size increases, more atoms become active and participate in the plastic deformation, leading to higher levels of ductility at the larger sizes. Clearly, this is due to the fact that smaller samples offer fewer opportunities for slip and dislocation motion, while larger specimens offer more opportunities for crystalline slip. This effect is clearly seen in Fig. 8.

4 CONCLUSION

Molecular dynamics simulations of the tensile deformation of single-crystal Cu nanowires are performed using an embedded atom method potential. The effects of

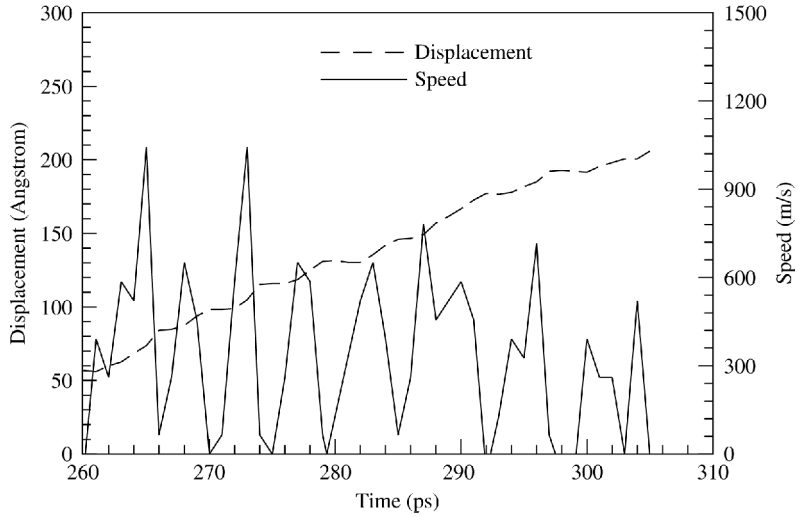

Fig. 5 Time histories of dislocation front displacement and velocity

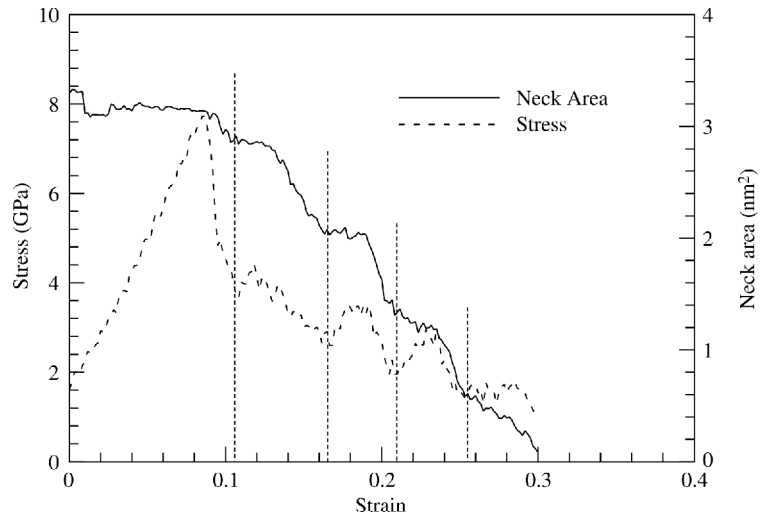

Fig. 6 Variation in stress and neck area of the nanowire during tensile deformation (size $5 \times 5 \times 60$, $\dot{\varepsilon} = 1.67 \times 10^9\ s^{-1}$)

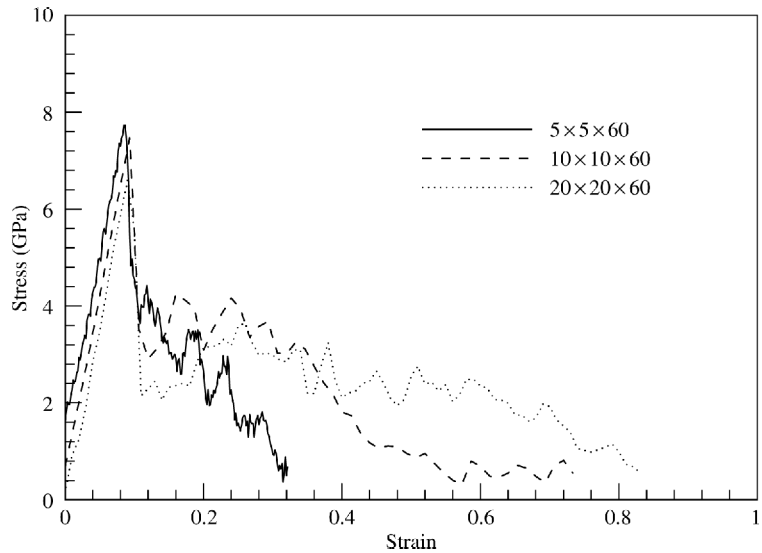

Fig. 7 Stress–strain relations for specimens of different sizes, $\dot{\varepsilon} = 1.67 \times 10^9\ s^{-1}$

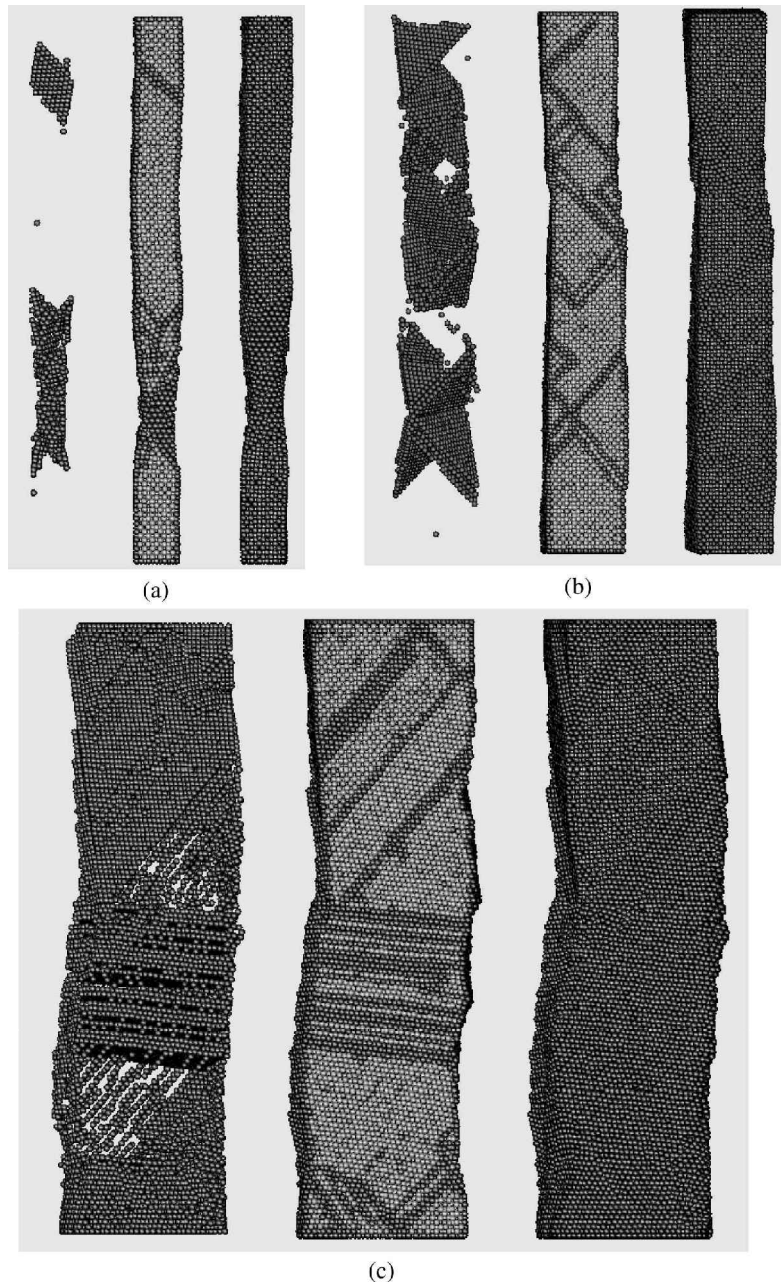

Fig. 8 Deformed configurations of Cu nanowires of different sizes ($\dot{\varepsilon} = 1.67 \times 10^9\ s^{-1}$): (a) specimen with a cross-sectional size of 5 lattice spacings ($\varepsilon = 9.17$ per cent); (b) specimen with a cross-sectional size of 10 lattice spacings ($\varepsilon = 18.3$ per cent); (c) specimen with a cross-sectional size of 20 lattice spacings ($\varepsilon = 23.3$ per cent)

strain rate and size scale are studied. Under the conditions analysed, the Young's modulus is found to be independent of strain rates and the cross-sectional size of the specimens. The yield stress decreases with specimen size and increases with loading rate. On the other hand, ductility increases with specimen size and strain rate. The influence of specimen size is a result of enhanced opportunities for dislocation motion at larger sizes. The influence of strain rate is due to the dynamic wave effect or phonon drag which impedes the motion of dislocations.

The analysis also focused on the variation in deformation mechanisms with specimen size and strain rate. There is a clear transition in the deformation mechanism as specimen size is changed. Specifically, when the cross-sectional dimensions are of the order of only a few lattice constants, crystalline slip on a pair of slip systems is observed. At larger cross-sectional sizes (10–20 lattice constants), cross-slip is primarily responsible for the progression of plastic deformation. Furthermore, a strong strain rate effect is also seen. As the strain rate is increased, a transition of the

deformation mechanism from sequential propagation of slip along well-defined and favourably oriented slip planes to amorphization is observed. The rapid occurrence of slip causes relaxation of stress over short times, resulting in an oscillatory stress–strain relation and decrease after yielding. At the lower strain rates, a well-structured activation of slip on alternating slip planes is the primary deformation mode.

ACKNOWLEDGEMENTS

This research was supported by NASA Langley Research Center. Computations were carried out at the NAVO and ERDC MSRCs. The authors would like to thank S. Plimpton for sharing his MD code. The images of deformation in this paper were created with the graphics package Visual Molecular Dynamics (VMD) {**14**}.

REFERENCES

1 **Agraït, N., Rubio, G.** and **Vieira, S.** Plastic deformation of nanometer-scale gold connective necks. *Phys. Rev. Lett.*, 1995, **74**(20), 3995–3998.

2 **Ikeda, H., Qi, Y., Cagin, T., Samwer, K., Johnson, W. L.** and **Goddard III, W. A.** Strain rate induced amorphization in metallic nanowires. *Phys. Rev. Lett.*, 1999, **82**(14), 2900–2903.

3 **Rubio-Bollinger, G., Bahn, S. R., Agrait, N., Jacobsen, K. W.** and **Vieira, S.** Mechanical properties and formation mechanisms of a wire of single gold atoms. *Phys. Rev. Lett.*, 2001, **87**(2), 026101–026104.

4 **Mehrez, H.** and **Ciraci, S.** Yielding and fracture mechanics of nanowires. *Phys. Rev. B*, 1997, **56**(19), 12632–12642.

5 **Cagin, T., Che, J., Qi, Y., Zhou, Y., Demiralp, E., Gao, G.** and **Goddard III, W. A.** *J. Nanoparticle Res.*, 1999, **1**(1), 51–69.

6 **Lu, L., Li, S. X.** and **Lu, K.** An abnormal strain rate effect on tensile behavior in nanocrystalline copper. *Scr. Mater.*, 2001, **45**, 1163–1169.

7 **Branicio, P. S.** and **Rino, J.-P.** Large deformation and amorphization of Ni nanowires under uniaxial strain: a molecular dynamics study. *Phys. Rev. B (Condensed Matter)*, 2000, **62**(24), 16950–16955.

8 **Horstemeyer, M. F.** and **Baskes, M. I.** Atomistic finite deformation simulations: a discussion on length scale effects in relation to mechanical stresses. *Trans. ASME, J. Engng Mater. Technol.*, 1999, **121**(2), 114–119.

9 **Nose, S.** A molecular dynamics method for simulations in the canonical ensemble. *Mol. Phys.*, 1984, **52**(2), 255–268.

10 **Hoover, W. G.** Canonical dynamics: equilibrium phase-space distributions. *Phys. Rev. A*, 1985, **31**(3).

11 **Kelchner, C. L., Plimpton, S. J.** and **Hamilton, J. C.** Dislocation nucleation and defect structure during surface indentation. *Phys. Rev. B (Condensed Matter)*, 1998, **58**(17), 11085–11088.

12 **Stalder, A.** and **Durig, U.** Study of yielding mechanics in nanometer-sized Au contacts. *Appl. Phys. Lett.*, 1995, **68**(5), 637–639.

13 **Branício, P. S.** and **Rino, J. P.** Large deformation and amorphization of Ni nanowires under uniaxial strain: a molecular dynamics study. *Phys. Rev. B (Condensed Matter)*, 2000, **62**(24), 16950–16955.

14 **Humphrey, W., Dalke, A.** and **Schulten, K.** VMD—visual molecular dynamics. *J. Molec. Graphics*, 1996, **14**(1), 33–38.